Available online at www.sciencedirect.com

SciVerse ScienceDirect

Solar Energy 86 (2012) 2106–2115

SOLAR ENERGY

www.elsevier.com/locate/solener

Dual-inverter for grid-connected photovoltaic system: Modeling and sliding mode control

V. Fernão Pires [a,b,*], J.F. Martins [c], Chen Hao [d]

[a] ESTSetúbal-Instituto Politécnico Setúbal/DEE, Setúbal, Portugal
[b] Center for Innovation in Electrical and Energy Engineering (CIEEE), Lisbon, Portugal
[c] CTS/UNINOVA and FCT/UNL, Lisbon, Portugal
[d] University of Mining and Technology, Xuzhou, China

Received 4 January 2012; received in revised form 2 April 2012; accepted 18 April 2012
Available online 10 May 2012

Communicated by: Associate Editor Mukund Patel

Abstract

A fast and robust control strategy for a multilevel inverter in grid-connected photovoltaic system is presented. The multilevel inverter is based on a dual two-level inverter topology. There are two isolated PV generators that feeding each bridge inverter. The output of each inverter is connected to a three-phase transformer. The active and reactive powers flowing into the grid are controlled by a sliding mode algorithm. An alfa–beta space vector modulator is also used. The inverters DC voltages are also controller by a sliding mode controller. In this way, a fast and robust system controller is obtained. Several test results are presented in order to verify the effectiveness of the proposed system controller.

Keywords: Photovoltaic system; Dual inverter; Sliding mode controller; Vector modulator; Power converter

1. Introduction

Photovoltaic systems had experienced a great amount of research and development work, making them a feasible alternative energy resource, on its own or complementing other energy sources in hybrid energy systems (either stand-alone or grid-connected). The trend of fast increase of the PV energy use is related to the increasing efficiency of solar cells as well as the improvements of manufacturing technology of solar panels and price reduction (solar photovoltaic systems today are more than 60% cheaper than they were in the 1990s). With the increasing development of renewable energies distributed generation systems, the renewable electricity from PV sources has become an important player. There are several research papers on the subject, and a good overview of interfacing topologies can be found at (Carrasco et al., 2006).

Many grid-connected photovoltaic systems use a three-phase inverter to perform this connection (Chaouachi et al., 2010; Yu et al., 2005; Kim, 2007). However, the classical three-phase inverter is very limited concerning its output voltage levels. It only allows obtaining three phase-to-phase output voltage levels. To overcome this problem, multilevel inverters have been proposed. There are several attractive features that make this kind of power converters very interesting for the power industry, such as, reduced current and voltage harmonics on the ac side, high voltage capability and low dv/dt's. The topology, modulation strategy and performance of these power converters have been extensively studied over the last decades. In this way several multilevel topologies have been proposed (Colak et al., 2011). The most used are the cascaded

* Corresponding author at: ESTSetúbal-Instituto Politécnico Setúbal/DEE, Setúbal, Portugal. Tel.: +351 265790000; fax: +351 265721869.
E-mail address: vitor.pires@estsetubal.ips.pt (V. Fernão Pires).

0038-092X/$ - see front matter
http://dx.doi.org/10.1016/j.solener.2012.04.012

H-bridge inverter (Hammond, 1997; Antunes et al., 2007), the neutral point clamped (Nabae et al., 1981), and the flying capacitor (Meynard and Foch, 1992). Due to this features many multilevel converters have been used for grid connected photovoltaic systems (Alonso-Martínez et al., 2010; Rahim et al., 2010; Ravi et al., 2011; Tsengenes and Adamidis, 2011).

In addition to the above attractive features of the multilevel inverters, in medium-power and high-power applications safety and robustness are also important. In this way isolated systems in low frequency are used. So, multilevel converters associate to line-frequency transformer have been proposed (Blaabjerg et al., 2004; Kang et al., 2005). One of the interesting multilevel topologies is the dual two-level inverter topology. The dual inverter connects to the primary of an open-end three-phase transformer.

There are several controllers for multilevel power converters, such as the sinusoidal PWM extended to multiple carrier arrangements (McGrath and Holmes, 2002). Other control techniques have also been used. Space vector modulation (SVM) is another strategy that has been extensively used. However, one of the fast and robust techniques is the sliding mode control (Gao and Hung, 1993). This control system has also been used to control power converters, such as, classical three-phase inverters, multilevel neutral point clamped and other power converters (Silva, 1999). The modelization of the power converters is also extremely important. This allows analyzing and developed many system controllers. In this way, many models for photovoltaic generators and their power converters have been presented (Ishaque et al., 2011; Kim et al., 2009).

In this work, it is presenting the modelization of the dual two-level inverter in grid-connected photovoltaic system. Due to the characteristics of the sliding mode control, the use of this control system is also proposed. Associated to this controller, an alfa–beta space vector modulator is also proposed. These systems will control the capacitors voltages and the output currents of the multilevel dual-inverter. These variables are controlled in order to control the active and reactive power that will flow to the grid. Standard control techniques use linear control theory (namely PI controllers) to regulate the capacitors voltages, which generate the amplitude of the reference currents (Green et al., 1988). Even the use of PWM modulators presents additional delays (Vilathgamura et al., 1996). In contrast with linear regulators, sliding-mode control is particularly interesting, besides its robustness and system order reduction, due to its suitability to the power switches' ON–OFF behavior.

The dual two-level inverter topology has also been used in other applications such as the control of an open-end winding induction motor (Stemmler and Guggenbach, 1993; Shivakumar et al., 2002) or the static synchronous compensator, STATCOM (Babu et al., 2011). Furthermore, this topology, based on cascaded two level inverters, has also been used for grid-connected photovoltaic systems with line-frequency transformer (Grandi et al., 2009). The control strategy proposed in this paper can also be used in the aforementioned applications. In the control of an open-end winding induction motor it is not necessary to control the capacitor voltage since both inverters are supplied by a DC voltage source. In this way, the system controller is simplified since it is only used to control the AC currents, being the references usually given in a dq referential. In the STATCOM application it is necessary to control, both, the AC currents and the DC capacitor voltage. In this way, the control strategy proposed in this paper can be used without any modification.

2. Model of the photovoltaic system

The grid connected photovoltaic system is composed by a PV string a DC/DC converter, two three-phase bridge inverters and three-phase low frequency transformer with the open winding configuration on primary side and secondary side connected to the grid (Fig. 1). The multilevel inverter based on two two-level three-phase voltage source inverter is presented in Fig. 2. This topology requires two isolated PV sources. Each PV source is connected to each of the inverter capacitors. At the output of the inverters is connected a three-phase transformer with the primary in open winding configuration.

2.1. PV array

The model of the PV array used in this system is based on the classical voltage–current characteristic equation of a solar cell (Gow and Manning, 1999; Simoes

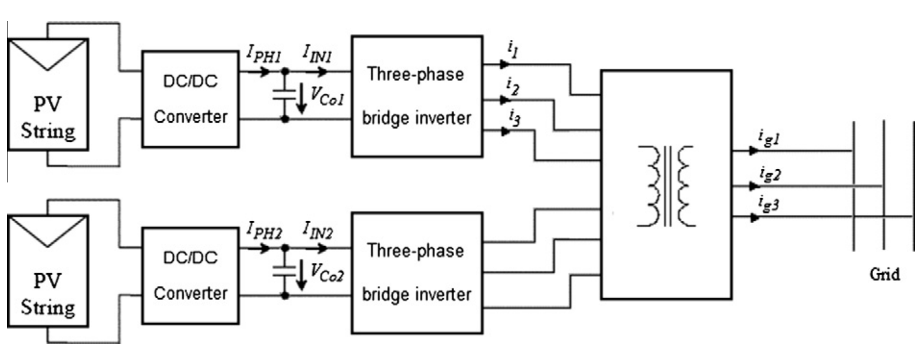

Fig. 1. Grid-connected photovoltaic system.

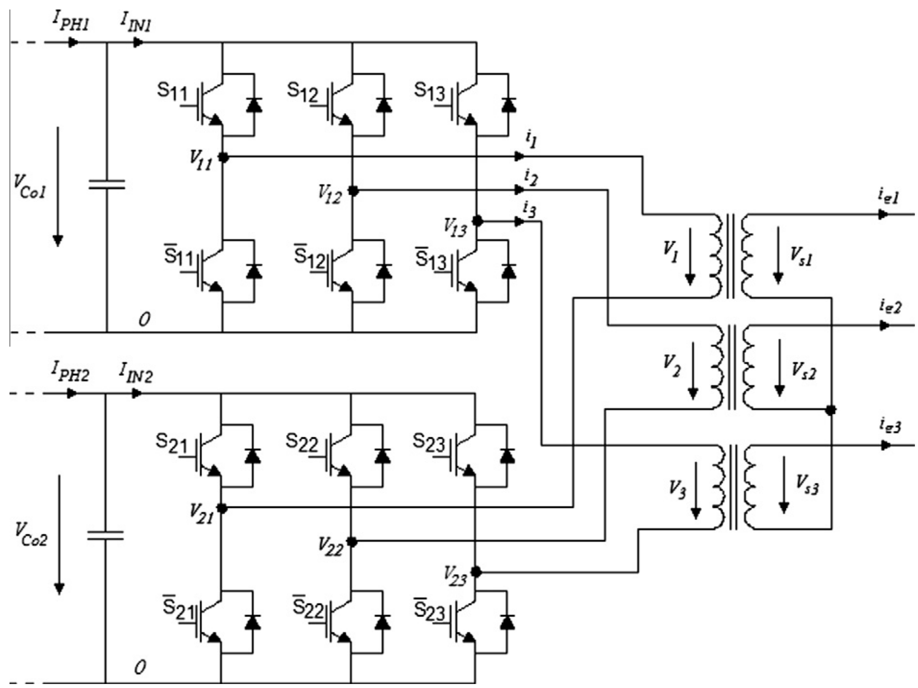

Fig. 2. Multilevel dual-inverter configuration.

et al., 2009). In this way, considering the standard current voltage-curve with 5 parameters the following current equation is given by:

$$I_{PH} = I_L - I_0\left[\exp\left(\frac{q(V + R_S I_{PH})}{nkTN_{cell}}\right) - 1\right] - \frac{V + R_S I_{PH}}{R_{sh}} \qquad (1)$$

where I_L denotes the current due to the solar radiation, I_0 the saturation current, q the electron charge, k the Boltzmann constant, T the temperature, R_S the series resistance, R_{sh} the shunt resistance, N_{cell} the number of series cells in a module and n the ideality factor ($n \in 1, 2$).

2.2. Dual-inverter model

To obtain the dual-inverter model, ideal power switches will be considered. In this way, according to Fig. 2, the following six switching functions α_{ij} $i \in \{1, 2\}$ $j \in \{1, 2, 3\}$ can be obtained:

$$\alpha_{ij} = \begin{cases} 1 & \text{if} \quad S_{ij} \text{ is ON} \wedge \overline{S}_{ij} \text{ is OFF} \\ 0 & \text{if} \quad S_{ij} \text{ is OFF} \wedge \overline{S}_{ij} \text{ is ON} \end{cases} \qquad (2)$$

Assuming ideal power switches, the output voltage of the dual-inverter is given by:

$$\begin{bmatrix} v_1 \\ v_2 \\ v_3 \end{bmatrix} = \frac{1}{3}\begin{bmatrix} 2 & -1 & -1 \\ -1 & 2 & -1 \\ -1 & -1 & 2 \end{bmatrix}\begin{bmatrix} v_{11} \\ v_{12} \\ v_{13} \end{bmatrix} - \frac{1}{3}\begin{bmatrix} 2 & -1 & -1 \\ -1 & 2 & -1 \\ -1 & -1 & 2 \end{bmatrix}\begin{bmatrix} v_{21} \\ v_{22} \\ v_{23} \end{bmatrix} \qquad (3)$$

where

$$\begin{cases} v_{1j} = \alpha_{1j} V_{Co1} \\ v_{2j} = \alpha_{2j} V_{Co2} \end{cases} \qquad (4)$$

Applying the Clark–Concordia transform (5), a new model for the output voltages can be obtained, as expressed by Eq. (6).

$$\begin{bmatrix} v_\alpha \\ v_\beta \end{bmatrix} = \sqrt{\frac{2}{3}}\begin{bmatrix} 1 & -\frac{1}{2} & -\frac{1}{2} \\ 0 & \frac{\sqrt{3}}{2} & -\frac{\sqrt{3}}{2} \end{bmatrix}\begin{bmatrix} v_1 \\ v_2 \\ v_3 \end{bmatrix} \qquad (5)$$

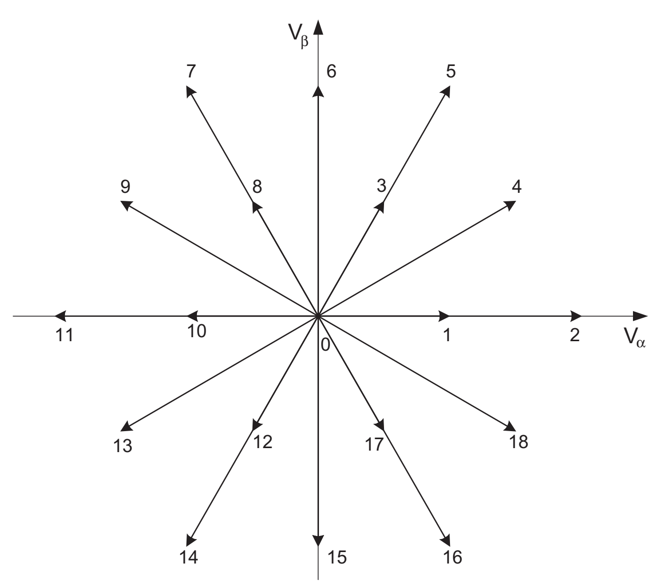

Fig. 3. Output voltage space-vectors of the dual inverter.

$$\begin{bmatrix} v_\alpha \\ v_\beta \end{bmatrix} = \begin{bmatrix} \sqrt{\frac{2}{3}} & -\frac{1}{\sqrt{6}} & -\frac{1}{\sqrt{6}} \\ 0 & \frac{1}{\sqrt{2}} & -\frac{1}{\sqrt{2}} \end{bmatrix} \begin{bmatrix} v_{11} \\ v_{21} \\ v_{31} \end{bmatrix} - \begin{bmatrix} \sqrt{\frac{2}{3}} & -\frac{1}{\sqrt{6}} & -\frac{1}{\sqrt{6}} \\ 0 & \frac{1}{\sqrt{2}} & -\frac{1}{\sqrt{2}} \end{bmatrix} \begin{bmatrix} v_{12} \\ v_{22} \\ v_{32} \end{bmatrix} \tag{6}$$

From this last model it is possible to verify, that considering $V_{Co1} = V_{Co2}$, and according to the switching states, 19 different output voltage levels can be obtained. Fig. 3 presents the dual inverter voltage vector plot in a $\alpha\beta$ space for the different output voltages:

Considering the transformer as an equivalent RL circuit, the following state space model of the dual inverter in the three-phase reference frame can be obtained:

$$\begin{aligned} \frac{d}{dt}\begin{bmatrix} i_1 \\ i_2 \\ i_3 \\ v_{Co1} \\ v_{Co2} \end{bmatrix} &= \begin{bmatrix} -\frac{R}{L} & 0 & 0 & 0 & 0 \\ 0 & -\frac{R}{L} & 0 & 0 & 0 \\ 0 & 0 & -\frac{R}{L} & 0 & 0 \\ 0 & 0 & 0 & 0 & 0 \\ 0 & 0 & 0 & 0 & 0 \end{bmatrix} \begin{bmatrix} i_1 \\ i_2 \\ i_3 \\ v_{Co1} \\ v_{Co2} \end{bmatrix} \\ &+ \begin{bmatrix} -\frac{2v_{Co1}}{3L} & \frac{v_{Co1}}{3L} & \frac{v_{Co1}}{3L} \\ \frac{v_{Co1}}{3L} & -\frac{2v_{Co1}}{3L} & \frac{v_{Co1}}{3L} \\ \frac{v_{Co1}}{3L} & \frac{v_{Co1}}{3L} & -\frac{2v_{Co1}}{3L} \\ \frac{i_1}{C_{o1}} & \frac{i_2}{C_{o1}} & \frac{i_3}{C_{o1}} \\ -\frac{i_1}{C_{o2}} & -\frac{i_2}{C_{o2}} & -\frac{i_3}{C_{o2}} \end{bmatrix} \begin{bmatrix} \alpha_{11} \\ \alpha_{12} \\ \alpha_{13} \end{bmatrix} \\ &- \begin{bmatrix} -\frac{2v_{Co1}}{3L} & \frac{v_{Co1}}{3L} & \frac{v_{Co1}}{3L} \\ \frac{v_{Co1}}{3L} & -\frac{2v_{Co1}}{3L} & \frac{v_{Co1}}{3L} \\ \frac{v_{Co1}}{3L} & \frac{v_{Co1}}{3L} & -\frac{2v_{Co1}}{3L} \\ \frac{i_1}{C_{o1}} & \frac{i_2}{C_{o1}} & \frac{i_3}{C_{o1}} \\ -\frac{i_1}{C_{o2}} & -\frac{i_2}{C_{o2}} & -\frac{i_3}{C_{o2}} \end{bmatrix} \begin{bmatrix} \alpha_{21} \\ \alpha_{22} \\ \alpha_{23} \end{bmatrix} \\ &+ \begin{bmatrix} \frac{1}{L} & 0 & 0 & 0 & 0 \\ 0 & \frac{1}{L} & 0 & 0 & 0 \\ 0 & 0 & \frac{1}{L} & 0 & 0 \\ 0 & 0 & 0 & -\frac{1}{C_{o1}} & 0 \\ 0 & 0 & 0 & 0 & -\frac{1}{C_{o2}} \end{bmatrix} \begin{bmatrix} v_{s1} \\ v_{s2} \\ v_{s3} \\ I_{PH1} \\ I_{PH2} \end{bmatrix} \end{aligned} \tag{7}$$

From Eq. (6) it is possible to verify that this model is non linear and time variant. In this way, applying a Park transformation (8), a new model denoted by Eq. (9) is obtained. This new model is also non linear but time invariant.

$$\begin{bmatrix} i_d \\ i_q \end{bmatrix} = \sqrt{\frac{2}{3}} \begin{bmatrix} \cos(\omega t) & \cos\left(\omega t - \frac{2\pi}{3}\right) & \cos\left(\omega t - \frac{2\pi}{3}\right) \\ \sin(\omega t) & \sin\left(\omega t - \frac{2\pi}{3}\right) & \sin\left(\omega t + \frac{2\pi}{3}\right) \end{bmatrix} \begin{bmatrix} i_1 \\ i_2 \\ i_3 \end{bmatrix} \tag{8}$$

$$\begin{aligned} \frac{d}{dt}\begin{bmatrix} i_d \\ i_q \\ v_{Co1} \\ v_{Co2} \end{bmatrix} &= \begin{bmatrix} -\frac{R}{L} & \omega & -\frac{\alpha_{d1}}{L} & \frac{\alpha_{d2}}{L} \\ -\omega & -\frac{R}{L} & -\frac{\alpha_{q1}}{L} & \frac{\alpha_{q2}}{L} \\ \frac{\alpha_{d1}}{C_{o1}} & \frac{\alpha_{q1}}{C_{o1}} & 0 & 0 \\ -\frac{\alpha_{d2}}{C_{o2}} & -\frac{\alpha_{q2}}{C_{o2}} & 0 & 0 \end{bmatrix} \begin{bmatrix} i_d \\ i_q \\ v_{Co1} \\ v_{Co2} \end{bmatrix} \\ &+ \begin{bmatrix} \frac{1}{L} & 0 & 0 & 0 \\ 0 & \frac{1}{L} & 0 & 0 \\ 0 & 0 & -\frac{1}{C_{o1}} & 0 \\ 0 & 0 & 0 & -\frac{1}{C_{o2}} \end{bmatrix} \begin{bmatrix} v_{sd} \\ v_{sq} \\ I_{PH1} \\ I_{PH2} \end{bmatrix} \end{aligned} \tag{9}$$

This last model will also be used to obtain the sliding mode controller for the dual inverter.

3. Maximum power point tracking

The power delivered by a PV system changes with the voltage and current across the array. So, in order to deliver the maximum power of a PV system, it is needed to implement a maximum power point tracking algorithm. Several maximum power point tracking algorithms have been developed. Among them, algorithms such as perturb & observe, incremental conductance, constant voltage and current, parasitic capacitor, sliding mode and fuzzy logic has been studied and presented. In this work, it was used the classic perturb & observe algorithm (Enrique et al., 2010; Chu and Chen, 2007; Messai et al., 2011). The output of this algorithm gives the duty cycle of the Boost converter.

4. Dual inverter controller

The goal of the system controller is to accomplish voltage regulation of the inverter capacitors. This is accomplished by controlling the active and reactive power that flows into the grid. Due to the characteristics of sliding mode controllers, such as response speed and robustness to external perturbations, this controlling methodology has been adopted. This sliding mode controller will be designed considering first a selected sliding surface and then the control law driving the state of the system onto the sliding surface.

From Eq. (9) it possible to verify that capacitors voltages can be controlled by acting in the inverters switches (variables γ_{d1}, γ_{d2}, γ_{q1} and γ_{q2}). However, capacitors voltages are also controlled by the three-phase output currents. In this way, considering inverter output currents and voltage capacitors as controlled outputs, the system dynamic equations written in phase canonical form are

$$\frac{d}{dt}\begin{bmatrix} i_q \\ v_{Co1} \\ \theta_1 \\ v_{Co2} \\ \theta_2 \end{bmatrix} = \begin{bmatrix} -\frac{R}{L}i_q - \omega i_d - \frac{\alpha_{d1}v_{Co1}}{L} + \frac{\alpha_{d2}v_{Co2}}{L} + \frac{v_{sq}}{L} \\ \theta_1 \\ -\frac{R}{L}\theta_1 - \frac{\alpha_{d1}^2+\alpha_{q1}^2}{LC_{o1}}v_{Co1} + \frac{\alpha_{d1}\alpha_{d2}+\alpha_{q1}\alpha_{q2}}{LC_{o1}}v_{Co2} + \frac{\omega(\alpha_{d1}i_q-\alpha_{q1}i_d)}{C_{o1}} + \frac{\alpha_{d1}v_{sd}+\alpha_{q1}v_{sq}}{LC_{o1}} - \frac{R}{LC_{o1}}I_{PH1} - \frac{1}{C_{o1}}\frac{dI_{PH1}}{dt} \\ \theta_2 \\ -\frac{R}{L}\theta_2 + \frac{\alpha_{d2}^2+\alpha_{q2}^2}{LC_{o2}}v_{Co2} - \frac{\alpha_{d1}\alpha_{d2}+\alpha_{q1}\alpha_{q2}}{LC_{o2}}v_{Co1} - \frac{\omega(\alpha_{d2}i_q-\alpha_{q2}i_d)}{C_{o2}} - \frac{\alpha_{d2}v_{sd}+\alpha_2 v_{sq}}{LC_{o2}} - \frac{R}{LC_{o2}}I_{PH2} - \frac{1}{C_{o2}}\frac{dI_{PH2}}{dt} \end{bmatrix} \tag{10}$$

where

$$\begin{bmatrix} \theta_1 \\ \theta_2 \end{bmatrix} = \begin{bmatrix} \frac{\alpha_{d1}i_d+\alpha_{q1}i_q-I_{PH1}}{C_{o1}} \\ \frac{-\alpha_{d2}i_d-\alpha_{q2}i_q-I_{PH2}}{C_{o1}} \end{bmatrix} \tag{11}$$

Analyzing Eq. (10) it is possible to verify that i_q current has a strong degree of zero (Gao and Hung, 1993), and capacitors voltage v_{Co1} and v_{Co2} have a strong degree of one. In this way, considering $i_{q\_ref} = 0$, and considering the feedback errors the following sliding surfaces can be obtained:

$$\begin{cases} S_1(e_{i_q}, t) = k_1(i_{q\,ref} - i_q) = 0 \\ S_2(e_{v_{Co1}}, e_{\theta 1}, t) = k_2(v_{Co1\,ref} - v_{Co1}) + k_3\left(\frac{dv_{Co1\,ref}}{dt} - \frac{dv_{Co1}}{dt}\right) = 0 \\ S_3(e_{v_{Co2}}, e_{\theta 2}, t) = k_4(v_{Co2\,ref} - v_{Co2}) + k_5\left(\frac{dv_{Co2\,ref}}{dt} - \frac{dv_{Co2}}{dt}\right) = 0 \end{cases} \tag{12}$$

From Eqs. (9) and (12), new sliding surfaces can be obtained as presented in the following equation.

$$\begin{cases} S_2(e_{v_{Co1}}, e_{\theta 1}, t) = k_2(v_{Co1\,ref} - v_{Co1}) + k_3\frac{dv_{Co1\,ref}}{dt} + k_3\frac{\alpha_{d1}i_d+\alpha_{q1}i_q}{C_{o1}} - k_3\frac{I_{PH1}}{C_{o1}} = 0 \\ S_3(e_{v_{Co2}}, e_{\theta 2}, t) = k_4(v_{Co2\,ref} - v_{Co2}) + k_5\frac{dv_{Co2\,ref}}{dt} + k_5\frac{\alpha_{d2}i_d+\alpha_{q2}i_q}{C_{o2}} - k_5\frac{I_{PH2}}{C_{o2}} = 0 \end{cases} \tag{13}$$

Based in steady-state power balance equations, and the fact that the steady state mean value of the capacitors current is zero, the following equations can be obtained:

$$\begin{cases} V_{Co1}I_{PH1} \approx v_d i_{d1} + v_q i_{q1} \\ V_{Co2}I_{PH2} \approx v_{d2}i_{d2} + v_{q2}i_{q2} \\ \alpha_{d1}i_{d1} + \alpha_{q1}i_{q1} \approx I_{PH1} \\ \alpha_{d2}i_{d2} + \alpha_{q2}i_{q2} \approx I_{PH2} \end{cases} \tag{14}$$

where $i_{d1} = i_d$, $i_{q1} = i_q$, $i_{d2} = -i_d$ and $i_{q2} = -i_q$.

Considering Eqs. (9) and (14) new sliding surfaces related with the capacitors voltage can also be obtained, as presented in the following equation.

$$\begin{cases} S_2(e_{v_{Co1}}, e_{\theta 1}, t) = k_2(v_{Co1\,ref} - v_{Co1}) + k_3\frac{dv_{Co1\,ref}}{dt} - k_3\frac{I_{PH1}}{C_{o1}} + k_3\frac{v_d}{V_{Co1}C_{o1}}i_{d1} = 0 \\ S_3(e_{v_{Co2}}, e_{\theta 2}, t) = k_4(v_{Co2\,ref} - v_{Co2}) + k_5\frac{dv_{Co2\,ref}}{dt} - k_5\frac{I_{PH2}}{C_{o2}} + k_5\frac{v_d}{V_{Co2}C_{o2}}i_{d2} = 0 \end{cases} \tag{15}$$

These sliding surfaces can be represented as difference between a i_{d_ref} and i_d as can be seen by the following equations:

$$\begin{cases} S_2(e_{v_{Co1}}, e_{\theta 1}, t) = i_{d1\_ref} - i_{d1} = 0 \\ S_3(e_{v_{Co2}}, e_{\theta 2}, t) = i_{d2\_ref} - i_{d2} = 0 \end{cases} \tag{16}$$

where

$$\begin{cases} i_{d1\_ref} = -\left[\frac{k_2 V_{Co1}C_{o1}(v_{Co1\,ref}-v_{Co1})}{k_3 v_d} + \frac{V_{Co1}C_{o1}}{v_d}\frac{dv_{Co1\,ref}}{dt} - \frac{V_{Co1}I_{PH1}}{v_d}\right] \\ i_{d2\_ref} = -\left[\frac{k_4 V_{Co2}C_{o2}(v_{Co2\,ref}-v_{Co2})}{k_5 v_d} + \frac{V_{Co2}C_{o2}}{v_d}\frac{dv_{Co2\,ref}}{dt} - \frac{V_{Co2}I_{PH2}}{v_d}\right] \end{cases} \tag{17}$$

To obtain sinusoidal currents the voltage controllers can only enforce the amplitude of the inverter currents that is injected to the grid and in phase with the grid. In this way, the sliding surfaces presented in (16) and (17) will only control the currents amplitude. Therefore, since the currents amplitudes are continuous variables a steady state will appear. So, the sliding surfaces related with the voltage capacitors will be increased by adding a new state variable, as can be seen by the following expression:

$$\begin{cases} i_{d1\_ref} = -\left[\frac{k_2 V_{Co1} C_{o1}(v_{Co1\,ref} - v_{Co1})}{k_3 v_d} + \frac{V_{Co1} C_{o1}}{v_d}\frac{dv_{Co1\,ref}}{dt} - \frac{V_{Co1} I_{PH1}}{v_d} + k_6 \int (v_{Co1\,ref} - v_{Co1})dt\right] \\ i_{d2\_ref} = -\left[\frac{k_4 V_{Co2} C_{o2}(v_{Co2\,ref} - v_{Co2})}{k_5 v_d} + \frac{V_{Co2} C_{o2}}{v_d}\frac{dv_{Co2\,ref}}{dt} - \frac{V_{Co2} I_{PH2}}{v_d} + k_7 \int (v_{Co1\,ref} - v_{Co1})dt\right] \end{cases} \tag{18}$$

From Eq. (18) it is possible to verify that the control strategy only depends on one system parameter (C_o). This parameter is multiplied by other values and, since it presents a very small value, its impact is very small.

Since the voltage capacitors are not always equal and the output three-phase currents of the inverter 1 is the input of the three-phase currents of the inverter 2, then the final current reference is the average value of i_{d1_ref} and i_{d2_ref}. Considering the final current reference i_{d_ref}, the inverse Park transformation (19) and $i_{q\_ref} = 0$ in (11) the final switching functions (20) can be obtained.

$$\begin{bmatrix} i_\alpha \\ i_\beta \end{bmatrix} = \begin{bmatrix} \cos(\omega t) & -\sin(\omega t) \\ \sin(\omega t) & \cos(\omega t) \end{bmatrix} \begin{bmatrix} i_d \\ i_q \end{bmatrix} \tag{19}$$

$$\begin{cases} S_\alpha(e_{i\alpha}, t) = (i_{d\_ref}\cos(\omega t) - i_{q\_ref}\sin(\omega t)) - i_\alpha = 0 \\ S_\beta(e_{i\beta}, t) = (i_{d\_ref}\sin(\omega t) - i_{q\_ref}\cos(\omega t)) - i_\beta = 0 \end{cases} \tag{20}$$

The control strategy must guarantee that the system trajectory moves towards and stays on the sliding surface from any initial condition. In order to achieve this strategy, the following stability condition must be achieved:

$$S_\alpha \quad (e_{i\alpha}, t)\dot{S}_\alpha(, e_{i\alpha}, t) < 0 \quad \text{and} \quad S_\beta \quad (e_{i\beta}, t)\dot{S}_\beta(e_{i\beta}, t) < 0 \tag{21}$$

To ensure the sliding surface (21), the switching law must be select according to the conditions expressed in the following equation.

Table 1
Output voltage vectors for the dual-inverter.

V_β	V_α								
	−1.6 V	−1.2 V	−0.8 V	−0.4 V	0	0.4 V	0.8 V	1.2 V	1.6 V
1.4 V	–	–	7	–	6	–	5	–	–
0.7 V	–	9	–	8	–	3	–	4	–
0	11	–	10	–	0	–	1	–	2
−0.7 V	–	13	–	12	–	17	–	18	–
−1.4 V	–	–	14	–	15	–	16	–	–

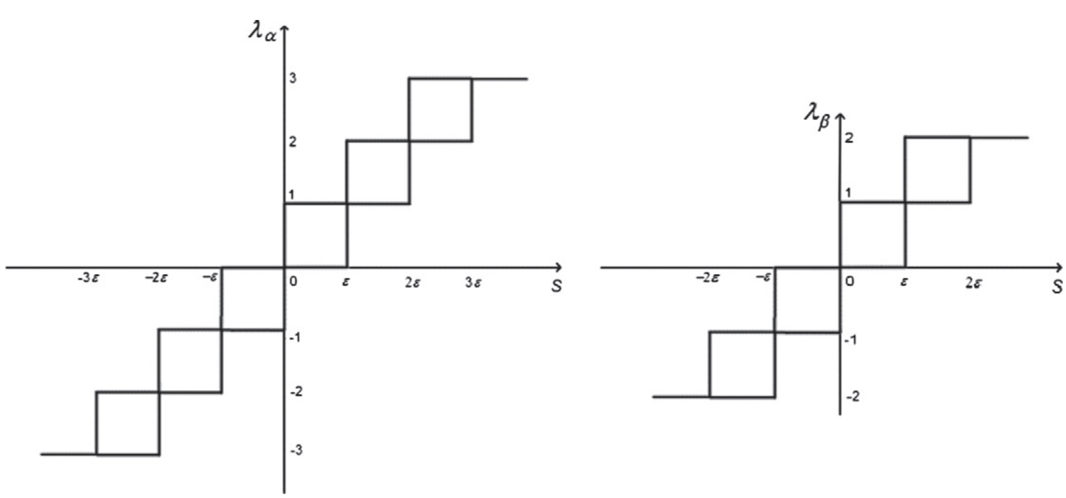

(a) seven level hysteretic comparator (b) five level hysteretic comparator

Fig. 4. Hysteretic comparators used at the output of the sliding mode controller.

$$\begin{cases} S_\alpha(e_{i\alpha},t) > 0 \Rightarrow \dot{\mathbf{S}}_1(e_{i\alpha},t) < 0 \Rightarrow i_\alpha > i_{\alpha_{ref}} \\ S_\alpha(e_{i\alpha},t) < 0 \Rightarrow \dot{\mathbf{S}}_1(e_{i\alpha},t) > 0 \Rightarrow i_\alpha < i_{\alpha_{ref}} \\ S_\beta(e_{i\beta},t) > 0 \Rightarrow \dot{\mathbf{S}}_1(e_{i\beta},t) < 0 \Rightarrow i_\beta > i_{\beta_{ref}} \\ S_\beta(e_{i\beta},t) < 0 \Rightarrow \dot{\mathbf{S}}_1(e_{i\beta},t) > 0 \Rightarrow i_\beta < i_{\beta_{ref}} \end{cases} \tag{22}$$

The condition expressed by (22) will be ensured by switching strategy. This strategy must select a specific dual-inverter output voltage. According to the state of the switches there are 19 different output voltage levels. Fig. 3 and Table 1 show the output voltage vectors that can be used in this power converter topology.

The number of voltage levels related with V_α is bigger than the number of voltage levels related with V_β. In this way, to implement this system, a seven-level and a five-level hysteretic comparators (with hysteresis ε in order to limit the maximum switching frequency) at the output of the sliding mode controller (20) is used. Fig. 4 presents these two hysteretic comparators. The output of these comparators are the integer variables λ_α and λ_β ($\lambda_a \in \{3,2;1;0;-1;-2,-3\}$, $\lambda_\beta \in \{2;1;0;-1;-2\}$) corresponding to seven and five selectable levels. These integer variables are related with the desired V_α and V_β voltages. According to variables λ_α, λ_β and Table 1 the switches that must be on are accurately selected.

5. Results

The multilevel dual-inverter with the proposed control system was implemented in Matlab/Simulink, using the SimPowerSystems toolbox. The voltages of the inverters capacitor have been set to 40 V. Fig. 5 shows the output voltage of the dual-inverter. From this figure it is possible to verify the multilevel operation of this power converter with the proposed controller. Fig. 6 shows the three-phase output currents of the dual-inverter. This figure shows that the current ripple is small. Since the grid voltage is synchronized with the output voltages of the dual-inverter, from

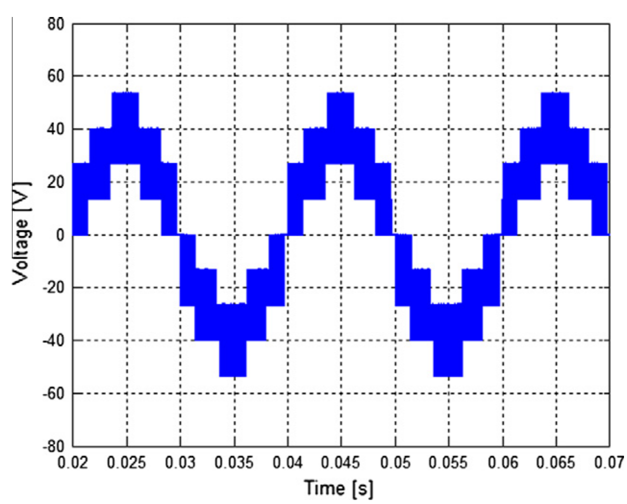

Fig. 5. Output voltage of the dual-inverter.

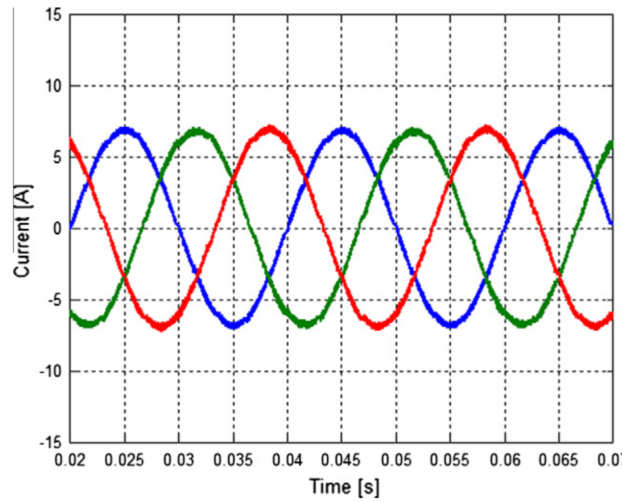

Fig. 6. Output currents of the dual-inverter.

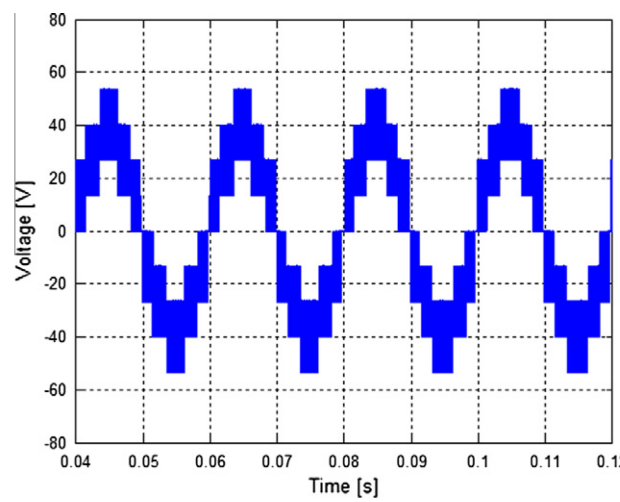

Fig. 7. Output voltage of the dual-inverter for a sudden change of the PV generator.

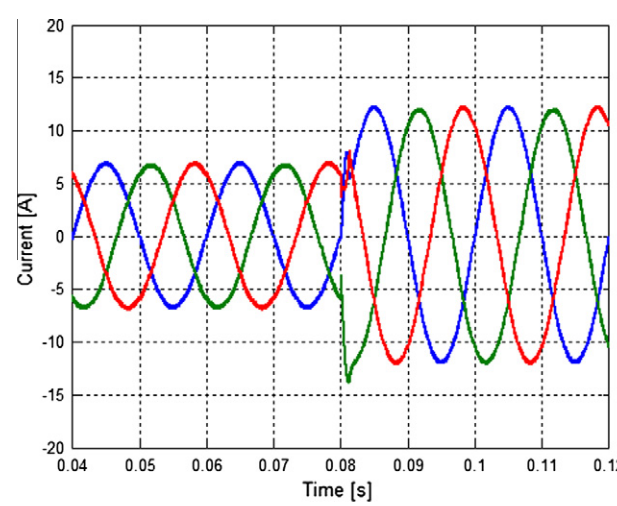

Fig. 8. Output currents of the dual-inverter for a sudden change of the PV generator.

these last two figures it is also possible to verify that the inverter output currents are in phase with the grid voltage.

Figs. 7 and 8 show the time behavior of the output voltage and currents of the dual-inverter for a sudden change of the PV generator. This sudden change is very fast in order to test the system controller. As can be seen by these figures, the system controller presents a fast response. The output voltage still presents the multilevel operation. The current amplitudes of the output currents suddenly increase in response to the change of the PV generator power. The ripple of the inverter output currents still remains very low. Fig. 9 shows the time behavior of the capacitor voltage V_{Co1}. From this figure it is also possible to verify the fast response of the system controller. At time 0.08 s there is a sudden change on the PV generator power, but the capacitor voltage practically maintains their initial value.

Figs. 10 and 11 show the time behavior of the capacitor voltage and three-phase currents of the dual-inverter for a sudden change in the voltage reference. At time 0.06 s the voltage reference increases with a step change from 40 V to 50 V, and at 0.12 s deceases with a step change from 50 V to 40 V. From these last figures it is possible to verify the fast response of the system controller. When the voltage reference changes from 40 V to 50 V the dual-inverter output currents will became zero. All the energy supplied by the PV generator will stored in the capacitors, until the capacitor voltage reach the desired value (50 V). When the capacitor voltage the output currents will change from zero to their final value (condition where all the energy supplied by the PV generators will be transferred to the grid). When the voltage reference changes from 50 V to 40 V the dual-inverter output currents will suddenly increase. In this situation, the energy that is transferred to the grid is the

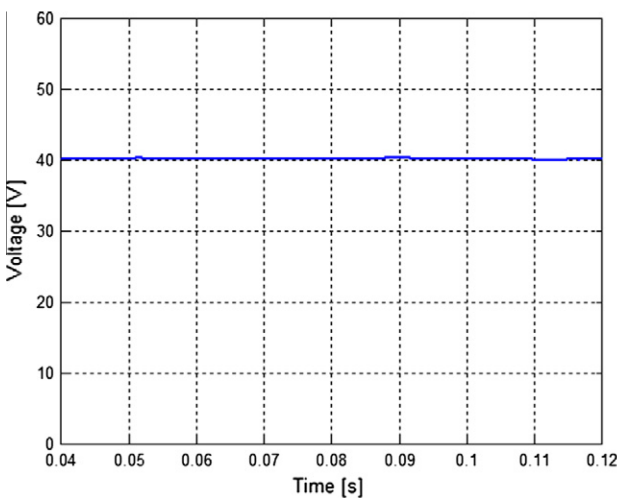

Fig. 9. Capacitor voltage of the dual-inverter for a sudden change of the PV generator.

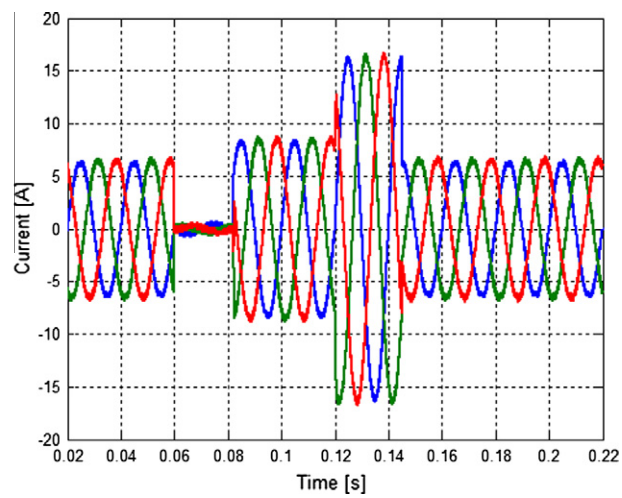

Fig. 11. Output currents of the dual-inverter for a sudden change of the reference voltage.

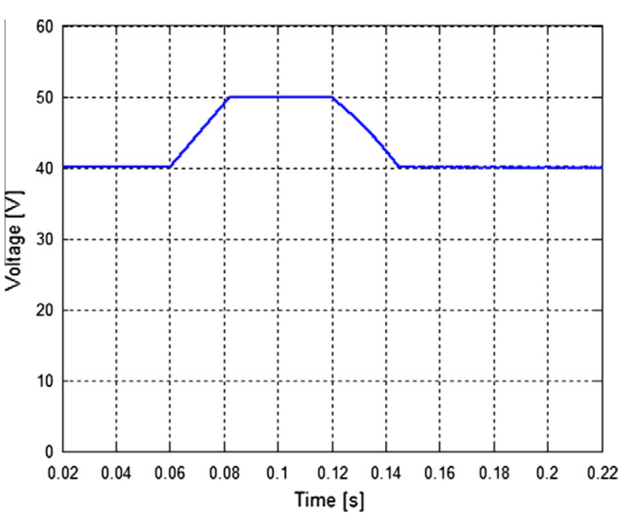

Fig. 10. Capacitor voltage of the dual-inverter for a sudden change of the reference voltage.

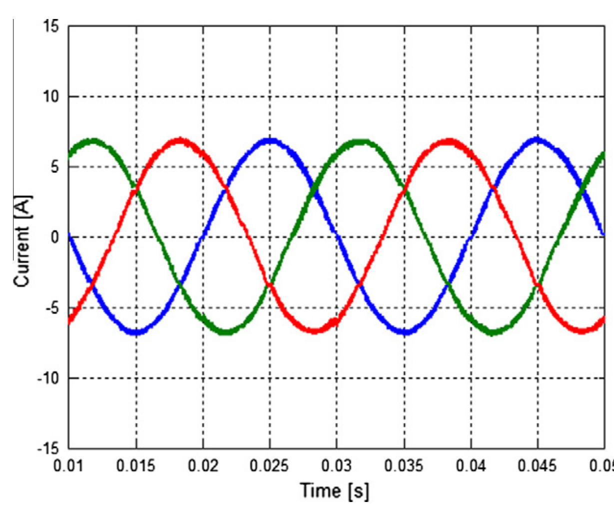

Fig. 12. Output currents of the dual-inverter for a sudden change of the control parameter C_o.

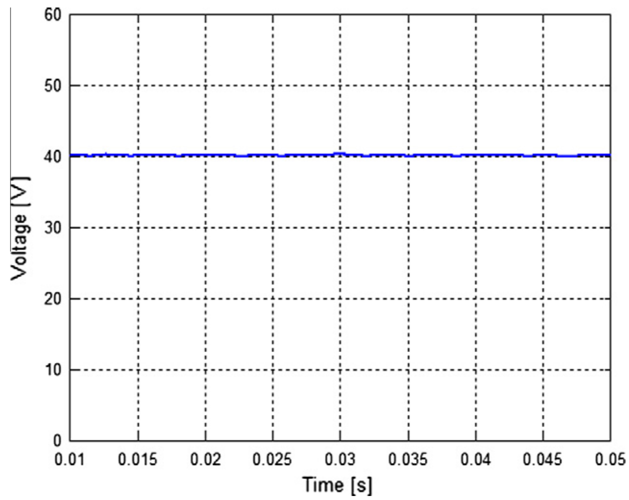

Fig. 13. Capacitor voltage of the dual-inverter for a sudden change of the control parameter C_o.

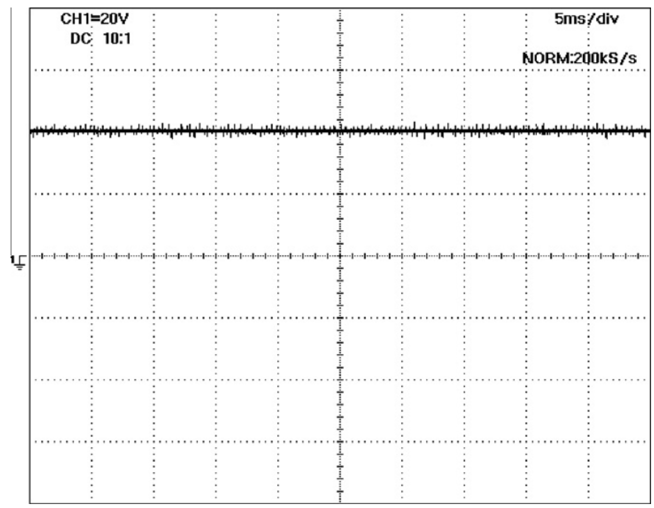

Fig. 16. Experimental result of the capacitor voltage.

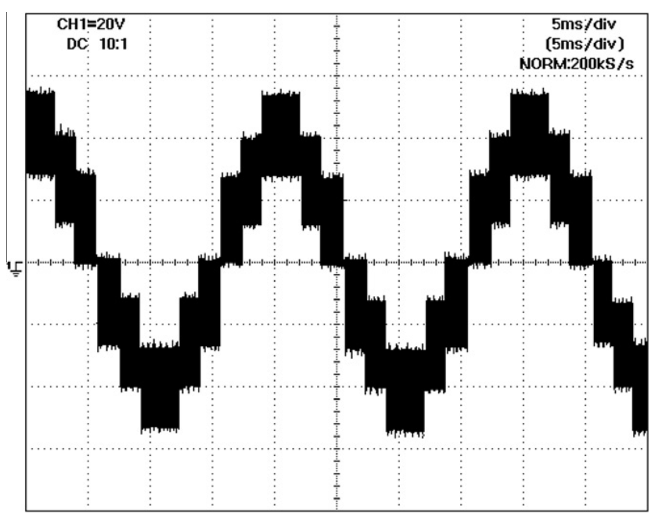

Fig. 14. Experimental result of the output voltage of the dual-inverter.

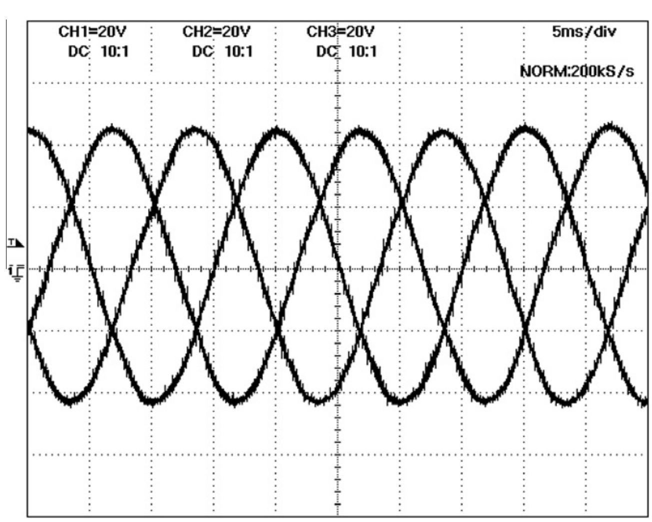

Fig. 15. Experimental result of the output currents of the dual-inverter.

sum of the energy from the PV generator and the capacitor storage energy. In this way, the capacitor will be discharged and rapidly decrease their voltage to the desired value. When the voltage capacitor reaches the reference voltage, the dual-inverter output currents will suddenly decrease to the final amplitude.

In order to verify the robustness of the system the following test, where the value of the system parameter C_o used in the sliding surface was changed, was conducted. Figs. 12 and 13 present the time behavior of the dual-inverter output currents and capacitor voltage V_{Co1} where, at time 0.03 s, a 15% change in the parameter value C_{o1} was considered. The obtained results show that this change does not have impact on the system's response.

A laboratory prototype was built in order to verify this system behavior in a real environment. Fig. 14 shows an experimental waveform of the dual-inverter output voltage, where the expected behavior can be confirmed, namely the multilevel operation of the power converter. Fig. 15 shows the experimental three-phase waveforms of the dual-inverter output currents. These currents are balanced with a low THD. Fig. 16 presents the experimental DC link voltage of the first power converter (V_{Co1}), where it is possible to confirm its stability.

6. Conclusions

A new system controller for the dual converter topology in grid-connected photovoltaic system has been presented. This topology uses two insulated PV generators and a three-phase open-end winding transformer. In this way, the system controller must perform the regulation of DC links in both sub converters. The proposed system controller uses a fast and robust sliding mode controller. The regulation of the voltage capacitors is obtained by the control of the inverter currents amplitude that is injected to the grid and in phase with the grid. For the generation of the proper multilevel waveforms a space-vector modulator was used. Since this topology allows obtaining 19 different output voltage vectors, a five and seven level comparators have been used to implement the sliding mode controller. The power converter system with the proposed controller has been implemented and verified by numerical simulations. From the obtained results it was possible to verify the effectiveness of the proposed control system. These results also show good performance both in steady state and transient conditions.

References

Alonso-Martínez, J., Eloy-García, J., Arnaltes, S., 2010. Direct power control of grid connected PV systems with three level NPC inverter. Solar Energy 84 (7), 1175–1186.

Antunes, V.M.E., Pires, V.F., Silva, J.F., 2007. Narrow pulse elimination PWM for multilevel digital audio power amplifiers using two cascaded H-bridges as a nine-level converter. IEEE Transactions on Power Electronics 22 (2), 425–434.

Babu, N.N.V.S., Rao, D.A., Fernandes, B.G., 2011. A new multilevel STATCOM based on cascaded two level inverters. In: International Conference on Power Engineering, Energy and Electrical Drives, pp. 1–6.

Blaabjerg, F., Teodorescu, R., Chen, Z., Liserre, M., 2004. Power converters and control of renewable energy systems In: Proc. Plenary Session Paper ICPE, p. 2.

Carrasco, J.M., Franquelo, L.G., Bialasiewicz, J.T., Galván, E., Portillo, R.C., Martín Prats, M.Á.J., León, E., Moreno-Alfonso, N., 2006. Power-electronic systems for the grid integration of renewable energy sources: a survey. IEEE Transactions on Industrial Electronics 53 (4), 1002–1016.

Chaouachi, A., Kamel, R.M., Nagasaka, K., 2010. A novel multi-model neuro-fuzzy-based MPPT for three-phase grid-connected photovoltaic system. Solar Energy 84 (12), 2219–2229.

Chu, C.-C., Chen, C.-L., 2007. Robust maximum power point tracker using sliding mode controller for the three-phase grid-connected photovoltaic system. Solar Energy 81 (3), 405–414.

Colak, I., Kabalci, E., Bayindir, R., 2011. Review of multilevel voltage source inverter topologies and control schemes. Energy Conversion and Management 52 (2), 1114–1128.

Enrique, J.M., Andújar, J.M., Bohórquez, M.A., 2010. A reliable, fast and low cost maximum power point tracker for photovoltaic applications. Solar Energy 84 (1), 79–89.

Gao, W., Hung, J., 1993. Variable structure control: a survey. IEEE Transactions on Industrial Electronics 40 (1), 2–22.

Gow, J.A., Manning, C.D., 1999. Development of a photovoltaic array model for use in power-electronics studies. IEE Proceedings – Electric Power Applications 146 (2), 193–200.

Grandi, G., Ostojic, D., Rossi, C., Casadei, D., 2009. A new multilevel conversion structure for grid-connected PV applications. IEEE Transactions on Industrial Electronics 56 (11), 4416–4426.

Green, A.W., Boys, J.T., Gates, G.F., 1988. Three-phase voltage source reversible rectifier. IEE Proceedings B 135 (6), 362–370.

Hammond, P.W., 1997. A new approach to enhance power quality for medium voltage AC drives. IEEE Transactions on Industry Applications 33 (1), 202–208.

Ishaque, K., Salam, Z., Syafaruddin, 2011. A comprehensive MATLAB Simulink PV system simulator with partial shading capability based on two-diode model. Solar Energy 85 (9), 2217–2227.

Kang, F.-S., Cho, S.E., Park, S.-J., Kim, C.-U., Ise, T., 2005. A new control scheme of a cascaded transformer type multilevel PWM inverter for a residential photovoltaic power conditioning system. Solar Energy 78 (6), 727–738.

Il-Song, Kim, 2007. Robust maximum power point tracker using sliding mode controller for the three-phase grid-connected photovoltaic system. Solar Energy 81 (3), 405–414.

Kim, S.-K., Jeona, J.-H., Choa, C.-H., Kima, E.-S., Ahn, J.-B., 2009. Modeling and simulation of a grid-connected PV generation system for electromagnetic transient analysis. Solar Energy 83 (5), 664–678.

McGrath, B.P., Holmes, D.G., 2002. Multicarrier PWM strategies for multilevel inverters. IEEE Transactions on Industrial Electronics 49 (4), 858–867.

Messai, A., Mellit, A., Guessoum, A., Kalogirou, S.A., 2011. Maximum power point tracking using a GA optimized fuzzy logic controller and its FPGA implementation. Solar Energy 85 (2), 265–277.

Meynard, T.A., Foch, H., 1992. Multi-level choppers for high voltage applications. European Power Electronics Journal 2 (1), 45–50.

Nabae, A., Takahashi, I., Akagi, H., 1981. A new neutral-point clamped PWM inverter. IEEE Transactions on Industry Applications IA–17 (5), 518–523.

Rahim, N.A., Selvaraj, J., Krismadinata, C., 2010. Five-level inverter with dual reference modulation technique for grid-connected PV system. Renewable Energy 35 (3), 712–720.

Ravi, A., Manoharan, P.S., Anand, J.V., 2011. Modeling and simulation of three phase multilevel inverter for grid connected photovoltaic systems. Solar Energy 85 (11), 2811–2818.

Shivakumar, E.G., Gopakumar, K., Sinha, S.K., Pittet, A., Ranganathan, V.T., 2002. Space vector control of dual inverter fed open-end winding induction motor drive. EPE Journal 12 (1), 9–18.

Silva, J.F., 1999. Sliding mode control of voltage sourced boost-type reversible rectifiers. IEEE Transactions on Industrial Electronics 46 (3), 594–603.

Simoes, J.P., Coelho, M.C., Pires, V.F., Martins, J.F., 2009. MATLAB/SIMULINK based teaching system for a Stand-Alone Energy System Supported by totally renewable hydrogen production. In: 3rd IEEE International Conference on E-Learning in Industrial, Electronics, pp. 86–91.

Stemmler, H., Guggenbach, P., 1993. Configurations of high-power voltage source inverter drives. In: 6th European Conference on Power Electronics and Applications vol. 5, pp. 7–14.

Tsengenes, G., Adamidis, G., 2011. A multi-function grid connected PV system with three level NPC inverter and voltage oriented control. Solar Energy 85 (11), 2595–2610.

Vilathgamura, D.M., Wall, S.R., Jackson, R.D., 1996. Variable structure control of voltage sourced reversible rectifiers. Proceedings of Institute of Electrical Engineering–Electrical Power Applications 143 (1), 18–24.

Yu, H., Pan, J., Xiang, A., 2005. A multi-function grid-connected PV system with reactive power compensation for the grid. Solar Energy 79 (1), 101–106.